



Ευρωπαϊκή Ένωση
Ευρωπαϊκό Ταμείο
Περιφερειακής Ανάπτυξης

ΕΛΛΗΝΙΚΗ ΔΗΜΟΚΡΑΤΙΑ
ΥΠΟΥΡΓΕΙΟ
ΟΙΚΟΝΟΜΙΑΣ & ΑΝΑΠΤΥΞΗΣ
ΕΙΔΙΚΗ ΓΡΑΜΜΑΤΕΙΑ ΕΠΠΑ & ΤΣ
ΕΙΔΙΚΗ ΥΠΗΡΕΣΙΑ ΔΙΑΧΕΙΡΙΣΗΣ ΕΠΑΝΕΚ

Με τη συγχρηματοδότηση της Ελλάδας και της Ευρωπαϊκής Ένωσης

ΕΠΑΝΕΚ 2014-2020
ΕΠΙΧΕΙΡΗΣΙΑΚΟ ΠΡΟΓΡΑΜΜΑ
ΑΝΤΑΓΩΝΙΣΤΙΚΟΤΗΤΑ
ΕΠΙΧΕΙΡΗΜΑΤΙΚΟΤΗΤΑ
ΚΑΙΝΟΤΟΜΙΑ



ΕΣΠΑ
2014-2020
ανάπτυξη - εργασία - αλληλεγγύη



Δράση ΕΡΕΥΝΩ – ΔΗΜΙΟΥΡΓΩ – ΚΑΙΝΟΤΟΜΩ

Συγχρηματοδότηση από την Ευρωπαϊκή Ένωση και τους εθνικούς πόρους μέσω του Ε.Π. Ανταγωνιστικότητα, Επιχειρηματικότητα & Καινοτομία (ΕΠΑΝΕΚ)

RADAR

“Ετερογενής Τρισδιάστατη Ολοκλήρωση με χρήση ρηξικέλευθων νανοτεχνολογιών για τη νέα γενιά μικροκυματικών πομποδεκτών ισχύος”

Κωδικός έργου: T1ΕΔΚ-00329

Ενότητα Εργασίας 2: ΣΧΕΔΙΑΣΜΟΣ & ΜΟΝΤΕΛΛΟΠΟΙΗΣΗ

Παραδοτέο 2.7 - M12

Ετήσιες δράσεις διάχυσης της ΕΕ2

Ημερομηνία : M12

Επικεφαλής παραδοτέου: ΣΝΔ

Συμμετέχοντες

ΙΤΕ: Γ. Κωνσταντινίδης

ΠΡΙΣΜΑ ΑΕ: Σ. Συμεωνίδης, Α. Καβουσανός-Καβουσανάκης, Χ. Ρομπίδου, Φ. Γιαννόπουλος

GLONATECH: Β. Βαμβακάς

INN: Π. Δημητράκης, Pascal Normand, Βασίλειος Ιωάννου-Σουγλερίδης

ΕΚΠΑ: Γ. Παπαϊωάννου, Δ. Μπιρμπιλιώτης, Μ. Κουτσουρέλη, Γ. Θεοχάρης

ΣΝΔ: Ε. Καραγιάννη, Ν. Μελανίτης, Χ. Βαζούρας, Ν. Φαφαλιός

ΑΜΕΝ: Δ. Νιάρχος, Κ. Καρυοφύλλης



Ευρωπαϊκή Ένωση
Ευρωπαϊκό Ταμείο
Περιφερειακής Ανάπτυξης



Με τη συγχρηματοδότηση της Ελλάδας και της Ευρωπαϊκής Ένωσης

ΕΠΑΝΕΚ 2014-2020
ΕΠΙΧΕΙΡΗΣΙΑΚΟ ΠΡΟΓΡΑΜΜΑ
ΑΝΤΑΓΩΝΙΣΤΙΚΟΤΗΤΑ
ΕΠΙΧΕΙΡΗΜΑΤΙΚΟΤΗΤΑ
ΚΑΙΝΟΤΟΜΙΑ



Περιεχόμενα

1. Αντικείμενο της Αναφοράς	2
2. Ιστότοπος “RADAR”	2
2.1. ΕΙΣΑΓΩΓΗ.....	2
2.2. ΣΧΕΔΙΑΣΜΟΣ, ΣΥΝΤΗΡΗΣΗ ΚΑΙ ΕΝΗΜΕΡΩΣΗ	2
2.3. ΔΙΑΦΘΩΡΩΣΗ ΙΣΤΟΣΕΛΙΔΑΣ	3
3. Δημοσιεύσεις σε διεθνή περιοδικά και συνέδρια (acknowledging RADAR)	5
3.1. Διεθνή Περιοδικά	5
3.2. Διεθνή Συνέδρια	8
4. Παρουσιάσεις σε διεθνείς επιστημονικές συναντήσεις	10

1. Αντικείμενο της Αναφοράς

Αντικείμενο της παρούσας αναφοράς είναι η καταγραφή των ενεργειών που έχουν γίνει κατά τη διάρκεια του πρώτου έτους του προγράμματος για τη διάχυση των αποτελεσμάτων της έρευνας στα πλαίσια της ΕΕ2 του PANTAP. Είναι αναμενόμενο η ποσότητα των ενεργειών αυτών να είναι σχετικά περιορισμένη για τους πρώτους 12 μήνες.

Αρχικά δημιουργήθηκε το ΙΤΕ ιστότοπος που είναι συνεχώς ενημερωμένος. Ο ιστότοπος παρουσιάζει τα προφίλ των εταιρών της κοινοπραξίας και τις δράσεις διάχυσης. Η τακτική προώθηση των ειδήσεων και των εκδηλώσεων του έργου γίνεται μέσω αυτού που θα παραμείνει ενεργός για τουλάχιστον τέσσερα ακόμη χρόνια.

Η κοινοπραξία φροντίζει τα αποτελέσματα να δημοσιεύονται σε περιοδικά μεγάλου αντικτύπου και να ανακοινώνονται σε σημαντικά διεθνή συνέδρια.

Επίσης, στόχος της κοινοπραξίας είναι η διάδοση των επιτευγμάτων του έργου σε διεθνή τεχνικά φόρουμ και σε ημερίδες στα πλαίσια των δράσεων της εθνικής υποδομής Innovation-EL και της ελληνικής επιστημονικής εταιρείας Micro & Nano. Επιπλέον θα γίνουν προσπάθειες για διάχυση προς τις σχετικές βιομηχανικές και ακαδημαϊκές οργανώσεις Public-Private Partnership (PPP clusters) της ΕΕ και άλλους φορείς όπως η European Defense Agency (EDA).

Η κοινοπραξία προτίθεται να οργανώσει θεματική ημερίδα για να διαφημίσει τα τεχνικά και επιστημονικά επιτεύγματα του έργου.

Οι δραστηριότητες προβολής του έργου και διάχυσης των αποτελεσμάτων του έργου περιλαμβάνουν και συμμετοχή σε εκδηλώσεις "ανοικτής ημέρας", παρουσιάσεις και ομιλίες κατά τη διάρκεια της "Βραδιάς του Ευρωπαίου Ερευνητή" και της "Μάθε περισσότερα, γίνε καλύτερος" εκπαιδευτικές δράσεις αφιερωμένες στα σχολεία. Φυλλάδια και δελτία θα παρουσιάζουν εκλαϊκευμένα τα αποτελέσματα του έργου στο ευρύ κοινό.

2. Ιστότοπος "RADAR"

2.1. ΕΙΣΑΓΩΓΗ

Ο ιστότοπος "RADAR" σχεδιάστηκε για να παρέχει πληροφορίες σχετικά με το έργο και για το πώς θα επιτευχθούν οι στόχοι του. Ο ιστότοπος του έργου "RADAR" διατίθεται στο <https://radar-project.iesl.forth.gr/> και είναι προσβάσιμο από κινητές συσκευές. Ο ιστότοπος σχεδιάστηκε για να αναθεωρεί και να αναπτύσσει συνεχώς τις δραστηριότητες διάδοσης στο πλαίσιο του έργου και να επιτρέπει συνεχή βελτίωση.

Ο δικτυακός τόπος περιλαμβάνει δύο διαφορετικούς τομείς, αφενός, έναν ιδιωτικό χώρο, ο οποίος χρησιμοποιείται κυρίως ως χώρος αποθήκευσης εγγράφων και ανταλλαγής διαβαθμισμένων πληροφοριών και, αφετέρου, δημόσιος χώρος. Ο δημόσιος χώρος του ιστότοπου θα προωθήσει το έργο "RADAR" μέσω σχετικών πληροφοριών, συμπεριλαμβανομένων των στόχων του έργου, του ιστορικού εταίρου και των μη ταξινομημένων αποτελεσμάτων του έργου.

Όλοι οι εταίροι θα συμμετάσχουν συλλογικά στην επικαιροποίηση διάδοσης της ιστοσελίδας παρέχοντας ενημερωμένες πληροφορίες

2.2. ΣΧΕΔΙΑΣΜΟΣ, ΣΥΝΤΗΡΗΣΗ ΚΑΙ ΕΝΗΜΕΡΩΣΗ

Ο ιστότοπος σχεδιάστηκε με έναν εύκολο τρόπο πλοήγησης, ο οποίος επιτρέπει στους χρήστες του ιστότοπου να μάθουν για το έργο και τα αποτελέσματά του, ειδήσεις κλπ. Όλα τα τμήματα του ιστότοπου έχουν στην κορυφή το λογότυπο RADAR (στα αριστερά) και μια αναφορά στη χρηματοδότηση εργαλεία (στα δεξιά).

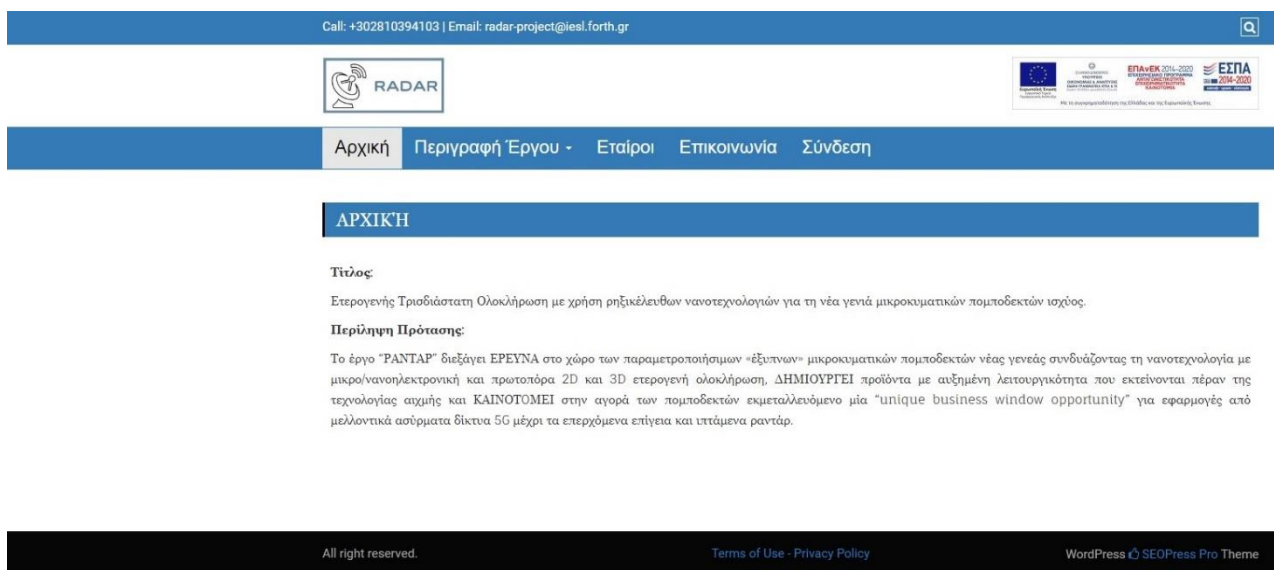


Η ιστοσελίδα φιλοξενείται και διοικείται από την Ομάδα Μικροηλεκτρονικής Έρευνας (MRG) του Ινστιτούτου Ηλεκτρονικής Δομής και Λείζερ (IESL) του Ιδρύματος Τεχνολογίας και Έρευνας (ΙΤΕ). Ένα αφοσιωμένο μέλος του προσωπικού της MRG επικαιροποιεί τακτικά τον ιστότοπο, μοιράζεται ειδήσεις, πληροφορίες σχετικά με εκδηλώσεις του έργου, παρουσιάσεις και άλλα σχετικά με το υλικό του έργου.

Ο ιστότοπος κατασκευάστηκε χρησιμοποιώντας το WordPress. Το WordPress είναι ένα ελεύθερο και ανοικτού κώδικα σύστημα διαχείρισης περιεχομένου (CMS) βασισμένο σε PHP και MySQL. Μεταξύ άλλων πλατφορμών, το Wordpress είναι μια δημοφιλής, καλά υποστηριζόμενη πλατφόρμα δημοσίευσης blogging και έχει μια μεγάλη κοινότητα που θα ελαχιστοποιήσει το ποσό της πολύπλοκης προσαρμογής που θα χρειαστεί να κάνει ο Συνεργάτης του Έργου.

2.3. ΔΙΑΡΘΡΩΣΗ ΙΣΤΟΣΕΛΙΔΑΣ

Ο δημόσιος χώρος έχει σχεδιαστεί για να εξασφαλίσει τη δημόσια προβολή των επιτευγμάτων και των αποτελεσμάτων του RADAR. Ο δημόσιος χώρος περιλαμβάνει πέντε κύριες σελίδες, όπως φαίνεται στο Σχήμα 1: Αρχική σελίδα, περιγραφή της εργασίας, συνεργάτες, διάδοση, επικοινωνία και μια καρτέλα "Σύνδεση" για να έχουν πρόσβαση οι συνεργάτες στην ιδιωτική περιοχή (προστατεύεται με κωδικό πρόσβασης). Αγγλικά είναι η γλώσσα που επιλέξατε.

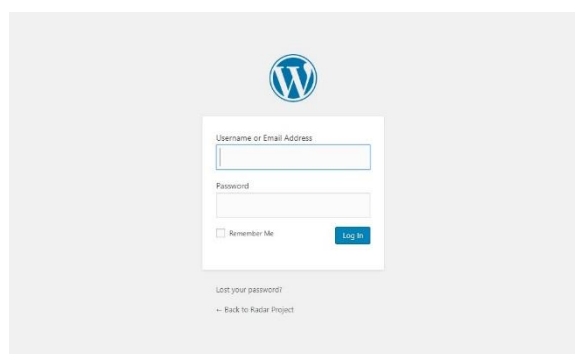


Σχήμα 1: Στιγμιότυπο οθόνης της αρχικής σελίδας του ιστότοπου "RADAR"

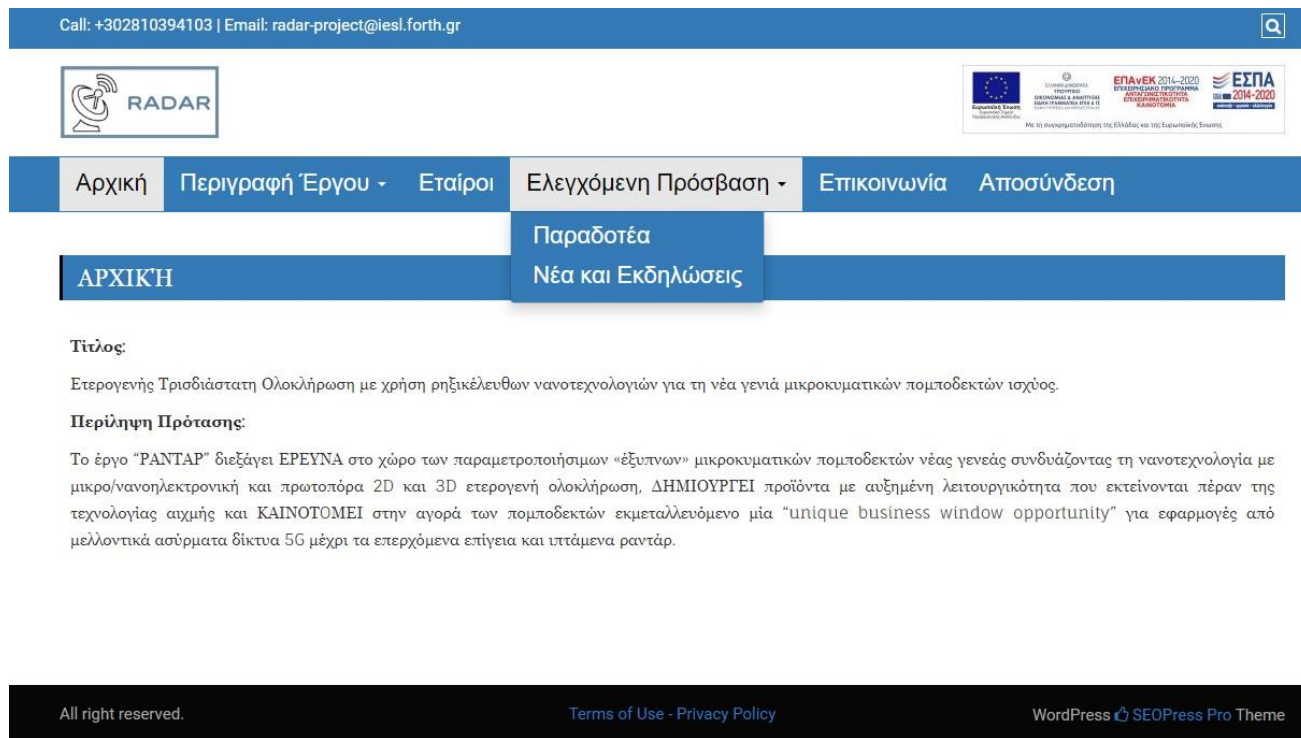
- Η σελίδα «**Αρχική**» παρέχει γενικές πληροφορίες για το έργο «RADAR».
- Η σελίδα «**Περιγραφή Έργου**» παρουσιάζει το αντικείμενο, τους στόχους και την μεθοδολογία υλοποίησης του έργου.
- Η σελίδα «**Εταίροι**» παρουσιάζει τις επωνυμίες των εταίρων που συμμετέχουν στο έργο, καθώς και τις συντομογραφίες μαζί με τις περιφέρειες του κάθε φορέα.
- Η σελίδα «**Επικοινωνία**» παρουσιάζει πληροφορίες (τηλέφωνα και διεύθυνση επικοινωνίας) που σχετίζονται με τον συντονιστή του προγράμματος.
- Η σελίδα «**Σύνδεση**» δίνει την δυνατότητα πρόσβασης στην ιδιωτική περιοχή του έργου «RADAR». Οι εταίροι ανακατευθύνονται στη σελίδα σύνδεσης και ζητούν τη σύνδεσή τους και τον κωδικό πρόσβασής τους για να μουν στην περιοχή.



Ο ιδιωτικός χώρος έχει σχεδιαστεί ως μια ενιαία πλατφόρμα εργασίας μόνο για εξουσιοδοτημένους χρήστες μόνο. Ο χώρος αυτός χρησιμοποιείται για την κοινή χρήση όλων των εμπιστευτικών εγγράφων και η πρόσβαση σε αυτήν απαιτεί διαδικασία σύνδεσης όπου όλοι οι εταίροι έχουν λάβει ο καθένας ξεχωριστά από ένα αναγνωριστικό ονόματος και κωδικό πρόσβασης. Στα παρακάτω Σχήματα 2 και 3 είναι στιγμιότυπα οθόνης της ιστοσελίδας του Έργου «RADAR».



Σχήμα 2: Για να έχει κάποιος χρήστη/εταίρος πρόσβαση στην ελεγχόμενη περιοχή της ιστοσελίδας, θα πρέπει να κάνει σύνδεση με χρήση ονόματος και κωδικού που του έχει δοθεί από τον διαχειριστή της ιστοσελίδας.



Σχήμα 3: Ο χρήστης/εταίρος της ιστοσελίδας όταν συνδεθεί επιτυχώς στην ελεγχόμενη περιοχή έχει πρόσβαση στις κατηγορίες «Παραδοτέα» και «Νέα και Εκδηλώσεις»

3. Δημοσιεύσεις σε διεθνή περιοδικά και συνέδρια (acknowledging RADAR)

3.1. Διεθνή Περιοδικά

1. Vassilios Constantoudis, George Papavlieros, Panagiotis Karakolis, Ali Khiat, Themistoklis Prodromakis and Panagiotis Dimitrakis, “Impact of Line Edge Roughness on ReRAM Uniformity and Scaling”, *Materials* 2019, 12, 3972; doi:10.3390/ma12233972



Article

Impact of Line Edge Roughness on ReRAM Uniformity and Scaling

Vassilios Constantoudis^{1,2,*}, George Papavlieros^{1,2,3}, Panagiotis Karakolis^{1,3}, Ali Khiat⁴, Themistoklis Prodromakis^{4,5} and Panagiotis Dimitrakis^{1,4,6}

¹ Institute of Nanoscience and Nanotechnology, NCSR Demokritos, 15341 Aghia Paraskevi, Greece; g.papav@inn.demokritos.gr (G.P.); p.karakolis@inn.demokritos.gr (P.K.)

² Nanometrisia P.C., 15341 Aghia Paraskevi, Greece

³ Department of Physics, University of Patras, GR 265 00 Patras, Greece

⁴ Electronic Materials and Devices Research Group, Zepher Institute for Photonics and Nanoelectronics, University of Southampton, Southampton SO17 1BJ, UK; ak112@ecs.soton.ac.uk (A.K.); T.Prodromakis@soton.ac.uk (T.P.)

⁵ Correspondence: v.constantoudis@inn.demokritos.gr (V.C.); p.dimitrakis@inn.demokritos.gr (P.D.)

Received: 29 September 2019; Accepted: 21 November 2019; Published: 30 November 2019



Materials 2019, 12, 3972

2 of 12

The uniformity of the cell SET and RESET voltages (V_{SET} and V_{RESET} , respectively) is a key-challenge to large-scale manufacturing of ReRAM technology. Up to now, it has been mainly related to the stochastic nature of conducting a filament creation process. Remedies that have been proposed consider (a) engineering of electrode/oxide interface [12], (b) inserting seeds (nanoparticles) in the oxide bulk [13], and (c) reduction of the size of cell area [14]. The latter is related to the scaling trends of ReRAM devices and is a great advantage of this technology since scaling down the dimensions of a ReRAM cell goes with the increase in performance uniformity due to the mitigation of stochastic filament formation. Thus, scalability is generally considered an advantage of ReRAM owing to the filamentary conduction and switching mechanisms. The effect of the reduction of the cell size area to the various parameters of ReRAM operation is an active matter of debate. To that end, in Reference [14] a simplified analytical model to describe the area and thickness scaling of forming voltage is proposed. Binary-oxide ReRAM scalability performance has drawn the attention of various groups. The general scaling trend of the high and low resistance states from various metal oxide ReRAMs has been presented in Reference [15]. The dependence of the scaling area on various ReRAM operation parameters (Resistance, SET/RESET current, SET/RESET voltage) has been studied thoroughly for HfO₂ [16,17], TaO_x [18], SiO₂ [19], ZnO₂ [20], and recently for Al₂O₃ [21] and for TiO₂ [22]. Similar scalability issues have been examined for perovskite material-based ReRAMs, such as SrTiO₃ [23], and metal nitrides, such as AlN [24] and NiN [25].

However, up to now no special attention has been paid on deviations from pattern's uniformity induced by the fabrication process and material properties. In CMOS technology, one of the most important sources of such deviations from manufacturing uniformity is related to the Line Edge Roughness (LER). LER is actually the sidewall roughness of pattern lines manufactured via standard lithographic rules, as often observed via top-down SEM images. The effect of LER becomes more evident as the size of devices is reduced, which is the reason for the recent upsurge of interest in LER control in modern <20 nm semiconductor manufacturing [26]. Obviously, LER is responsible for the area variability of devices in a crossbar (Xbar) array and, furthermore, the cell-to-cell and wafer-to-wafer variability that appear in the operation parameters of ReRAM memory cells in Xbar arrays. More specifically, as mentioned in [11], the resistance at HRS increases as the inverse of the area cell A (i.e., $R_{HRS} \sim 1/A$) while the reset current increases as A decreases. Furthermore, the reduction of the cell size A attributes to local heating causing faster switching times [17]. In addition, forming and SET voltages also increase as the cell area A decreases [17]. These detrimental LER effects are expected to become stronger increasing the size of the memory crossbar array: The larger the memory array the stronger the effects are.

The importance of LER is justified by the evaluation of its effects on device performance. This can be done through carefully designed experiments or modeling/simulation studies. Results from such studies help defining the specifications for allowed LER in roadmaps and factory production lines. Clearly, the level of acceptable LER is defined by the operating constraints of distinct applications that employ nanoscale devices. Up to now, several modeling and experimental investigations have been performed for conventional MOSFET [27–30] and FinFET [31,32] devices. On the contrary, very few studies have been devoted to the LER effects on memory and especially ReRAM devices. In the fabrication of ReRAM and especially in the cross-point configurations, the LER of metallic lines may affect device performance through the induced variability to the cross-point cell areas and consequently to the device resistance.

Furthermore, it was recently realized that LER characteristics are sensitive to the applied lithographic technique [33]. The main point of differentiation comes from the degree of correlations between the fabricated edges and lines. In EUV patterns, for example, the nearby lines and edges are totally uncorrelated while in Multiple Pattern (MP) techniques correlations are induced mainly between the edges of each line, whereas lines are still independent at least for Double Patterning (DP) schemes. On the contrary, in Directed Self-Assembly (DSA) lithography even nearby lines exhibit correlated fluctuations arising from the very self-assembly nature of the process and the sidewall

Abstract: We investigate the effects of Line Edge Roughness (LER) of electrode lines on the uniformity of Resistive Random Access Memory (ReRAM) device areas in cross-point architectures. To this end, a modeling approach is implemented based on the generation of 2D cross-point patterns with predefined and controlled LER and pattern parameters. The aim is to evaluate the significance of LER in the variability of device areas and their performances and to pinpoint the most critical parameters and conditions. It is found that conventional LER parameters may induce >10% area variability depending on pattern dimensions and cross edge/line correlations. Increased edge correlations in lines such as those that appeared in Double Patterning and Directed Self-assembly Lithography techniques lead to reduced area variability. Finally, a theoretical formula is derived to explain the numerical dependencies of the modeling method.

Keywords: Resistive Random Access Memory (ReRAM); Line Edge Roughness (LER); variability; uniformity; modeling; lithography

1. Introduction

Resistive Random Access Memory (ReRAM) technologies are considered as one of the most promising candidates for future nonvolatile memory (NVM) applications due to their high memory capacity [1], their simple two-terminal architecture, and their excellent scalability [2]. ReRAM cells can be programmed faster than current NVMs and at lower voltages, overall leading to a significant reduction in energy consumption per bit [3]. The cross-point metal-insulator-metal (MIM) cell simple structure requires very low thermal budget and thus can be integrated easily in the current CMOS Back End of Line (BEOL) processing steps [4]. Large memory blocks have been implemented and demonstrated, following the cross-point architecture [5]. The cross-point area $F \times E$ is the lithography node, can be as small as $2 \text{ nm} \times 2 \text{ nm}$ [6] leading to a very small cell footprint (area/bit) $4E^2$. Conductive AFM experiments have demonstrated that the ReRAM memory cell area can be as small as that of an AFM tip [7]. In addition, the 3D stacking of different memory layers [8] reduces the cell's footprint to $4E^2/n$, where n is the number of the stacked memory layers, and hence severely increases the density of the ReRAM memory chips. Moreover, the ReRAM cell can be used to realize memristive devices to implement new computing paradigms like neuromorphic [3,9], reconfigurable electronics [10], and logic-in-memory [11].

roughness of grapho-epitaxy grating used for the alignment of lines. Therefore, LER modeling should always consider such aspects and adjust the modeled patterns according to the considered lithography. Up to now, the modeling strategies for the generation of line edges similar to the fabricated ones are based on inverse Fourier techniques, where no correlations are taken into account between edges or lines [34,35].

In order to get a better picture of the LER impact on cell area uniformity, one can observe Figure 1a where several ReRAM prototypes, of cross-point architecture, were fabricated by e-beam lithography and are depicted in a top-down SEM image. Furthermore, on the same SEM image the detected edges defining the borders of electrode lines are illustrated with black color. It can be clearly seen that the roughness of the metal edges induces non-uniform cell areas (see Figure 1b). The distribution of the cell areas is presented in Figure 1c where one can notice the wide distribution of cell area values. This data supports our claim that LER needs to be considered carefully for achieving a uniform and reliable ReRAM technology and deserves more investigation.

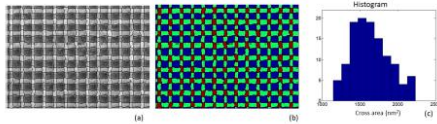


Figure 1. (a) A top-down SEM image of a cross-point pattern with the detected edges of the vertical and horizontal metal lines defining the crossing areas, (b) a colored illustration of the SEM image to show the crossing areas more clearly in red color and the metal lines in green color, (c) the histogram of the calculated cross-point area values in nm². The Line Edge Roughness (LER) (average root mean square (rms) value) of the vertical and horizontal lines was measured and found equal to 2.6 and 3.8 nm, respectively. The width of the distribution of cross areas (standard deviation) is found to be almost 16% of the mean value. Therefore, the commonly used three times this value reaches almost 50% of the mean value indicating the strong impact of LER of metal lines to the nonuniformity of Resistive Random Access Memory (ReRAM) device areas.

In this paper, we evaluate the effects of LER of metallic lines on the device area uniformity, which is critical for the device performance. Three types of line patterns are considered corresponding to EUV, Multiple Patterning (MP), and DSA patterns to compare these with respect to their vulnerability to LER defect. In Section 2, the modeling methodology is presented and explained. The results of the modeling approach to EUV, MP, and DSA-based patterns are shown and discussed in Section 3. In the end of the same section, we also derive an analytical formula capturing the numerical modeling results with quantitative success. The last section, Section 4, summarizes the findings of the paper and draws the main conclusions.

2. Modeling Methodology

2.1. Background of Modeling LER Characterization in Different Lithography Techniques

LER is usually defined as the deviation from smoothness (flatness) of the sidewalls of resist or substrate lines. In top-down SEM images, this deviation is reflected through the roughness of the edge defining the 2D borders of the line region. In the initial stages of LER studies, line edge points were considered uncorrelated and the main emphasis was given on the measurement of their root mean square (rms) value (standard deviation), quantifying the wideness of the edge point distribution. However, quite early, the characterization scheme was enriched with more parameters and functions

aiming to capture and quantify the spatial/lateral or frequency aspects of LER preserving the dominant significance of rms. To this end, a three-parameter model has been proposed [26] consisting of rms value, correlation length ξ , and roughness exponent α (related to the fractal dimension $d = 2 - \alpha$) and extensively used in different applications. The first parameter rms quantifies the vertical aspects of LER and is calculated by the standard deviation of the edge points about their mean value. The other two parameters (ξ and α) focus on the spatial aspects of LER. The correlation length ξ quantifies the window inside which the edge points can be considered correlated, i.e., they have similar deviations from the mean value, and delivers a statistical estimation of the mean width of edge fluctuations. Large values of ξ mean slowly varying edges while small values characterize more jagged edges. The correlation length is normally calculated through the autocorrelation function $R(r)$ as the distance r at which $R(r)$ is lowering beneath $1/e$, i.e., $R(\xi) = 1/e$ [36]. The roughness exponent $0 < \alpha < 1$ quantifies the contribution of various scales and frequencies to the whole LER. When α takes on low values, high frequencies dominate, whereas when it approaches 1, the edge becomes smoother at small scales and the importance of high frequency fluctuations is being lessened.

When a more detailed function-like characterization of spatial and frequency LER aspects is demanded, the Power Spectrum (PS) and the Height-Height Correlation Function (HHCF) can be calculated and elaborated. The overall shape of these functions is linked to the three-parameter model, when LER obeys a self-affine fractal symmetry [36]. The effects of LER on line width fluctuations (usually called Line Width Roughness (LWR)) complete the overall picture of the conventional approach to LER metrology. The relationship between LER and LWR metrics has been clarified and it can be shown that the low frequency LWR could have a significant contribution to the total budget of local Critical Dimension Uniformity (CDU). This effect has underlined the importance of estimating the PS of LWR, which quantifies the contribution to LWR from different frequency areas. A detailed presentation of the conventional LER and LWR metrology can be found in [26].

Nevertheless, during the recent years significant changes in lithographic landscape have been evidenced. The conventional scaling down of feature dimensions, based on the optimization of wavelength and Numerical Aperture (NA), has been replaced by a more etch-based and material-driven resolution enhancement, which duplicates the density of patterns through successive deposition and etching steps. The family of these MP techniques is currently used in high volume manufacturing in semiconductor industries. Additionally, the concept of self-assembly of block copolymers has been employed in lithography research in the last 10 years due to its ability to easily provide line/space patterns with widths less than 20 nm. The DSA lithography has seen an upsurge and very important advances have been performed in defect reduction and scaling improvement. However, what is usually missing is the effect that these new lithographic approaches have on LER and its metrology characterization. The key aspect of these effects is the lateral (across line direction) correlations they introduce in line/space patterns. In the EUV lithography patterns, the LER of edges are uncorrelated and no propagation of edge fluctuations is noticed between the edges of a line or the nearby lines of a pattern. On the contrary, in MP lithography patterns, the edges of the same line fluctuate in a correlated manner forming wiggling lines. A more dramatic change is observed in DSA patterns. Here, not only the line edges but also the lines themselves present correlations in the way they fluctuate. To capture these new aspects of LER, an extended framework for LER/LWR metrology has been proposed and elaborated based on the c-factor parameter, function, and correlation length. A detailed presentation and examples of application of these metrics can be found in [35].

2.2. Implementation of Modeling

The key idea of our approach is to model LER effects in cross-point area statistics using the 2D projections of the real 3D patterns, as they are shown in top-down SEM images similar to that in Figure 1. The assumption behind this approach is that 3D morphological variations do not have an important contribution to LER impact on device variability. This assumption is supported by

recent observations according to which the sidewall roughness of lithographic lines does not change significantly along z-direction since it exhibits a curtain-like morphology [37].

The modeling methodology is implemented in three steps. First, the structural parameters of the cross-point pattern are defined including line width (Critical Dimension, CD) and pitch values. The numbers of both vertical and horizontal lines are included in the modeling as well as. These parameters can differ in vertical (y) and horizontal (x) line patterns, though throughout this study we mainly consider the symmetrical case where $CD_x = CD_y$ and $pitch_x = pitch_y$. Based on these parameters, the ideal smooth pattern can be generated as shown in Figure 2a. In the second step, the smooth edges are converted to rough edges characterized by the input predetermined roughness parameters: rms, ξ , and α . The generation of rough edges is made using the convolution method and requires the use of a model function for the Power Spectrum or the Height-Height Correlation Function. Here, we extensively use the following HHCF $G(r)$ that is also used in self-affine rough processes [34,38]:

$$G^2(r) = 2rms^2(1 - e^{-r/\xi})^\alpha. \quad (1)$$

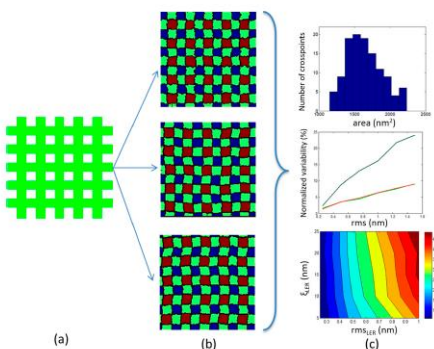


Figure 2. A schematic view of our modeling steps for LER effects on device uniformity. First, a pattern is formed (a) with the given parameters (Critical Dimension (CD), pitch, number of lines), then (b) roughness is imposed on the edges to get LER with predefined parameters, and then in (c) the statistical analysis of cross areas A_i is performed to get the normalized standard deviation $\sigma(A)$ versus LER parameters.

The successive application of the convolution method with no further processing of edges produces uncorrelated edges, which then can be positioned according to CD and pitch values to build the whole cross-point pattern. The generated pattern can be used to model the 2D projection of line/space

structures fabricated by mask-based lithographic rules (EUV or 193). When MP or DSA patterns are sought, we may add correlation either between the edges of the same line or to expand these between nearby lines to get DSA-like patterns. Figure 2b shows examples of such patterns with controlled LER parameters as well as cross-edge and cross-line correlations.

In the third step of our methodology, we measure the areas of cross-points A_i , $i = 1, \dots, N_x N_y$, where horizontal and vertical lines overlap in the considered rough pattern of $N_x \times N_y$ lines. Then we calculate the normalized standard deviation $\sigma(A)$ of the A_i values ($\sigma(A) = \text{std}(A_i) / A_i > 0$) and we plot it for various dimensional and LER parameters and edge/line correlation levels (see Figure 2c).

3. Results and Discussion

The results of our modeling calculations are collectively illustrated in Figure 3, which displays six contour plots. Each one of these plots depicts the dependence of $\sigma(A)$ on the LER parameters rms and ξ given that these parameters are considered to quantify LER according to the last editions of ITRS [39]. In all runs, the roughness exponent α is kept fixed to 0.5 in conformity with more experimental measurements. We consider that both horizontal and vertical lines have similar LER parameters. The left column of Figure 3a,c,e contains the contour plots with $CD = 20$ nm and $pitch = 40$ nm while the right column shows the results when the pattern scales down at $CD = 10$ nm and $pitch = 20$ nm. The different rows account for increased levels of horizontal (cross-line) correlations between edges and lines. In the first row, both edges and lines are generated to be uncorrelated to capture the case of mask lithography line structures (EUV and 193). The second row contains the results for cross-point patterns where the edges of each line are correlated, though the lines themselves fluctuate independently. The latter pattern resembles the line/space structures acquired by Double Patterning Lithography techniques. In the third row, the contour plots concern model patterns where the horizontal correlations propagate across both edges and lines similarly to what is happening in DSA.

From the contour plots of Figure 3, we are able to extract conclusions and discuss the following issues: (a) the dependence of $\sigma(A)$ on LER parameters rms and ξ which seems to exhibit a similar pattern in all cases, (b) the effects of scaling down the pattern dimensions, and (c) the effects of cross-edge and line correlations.

3.1. The Impact of LER Parameters Rms, ξ

The overall shape of all contour plots in Figure 3 is characterized by the dominance of vertical contour lines, which reveal the stronger dependence of area uniformity on rms with respect to that of the correlation length. In order to focus on the dependencies themselves, we take a horizontal and vertical cross-section of the contour diagrams and the outcome plots are shown in Figure 4 for all considered cases. One can easily notice the linear increase of $\sigma(A)$ with rms value in all cases, while the effects of ξ are sublinear justifying the dominant role of rms in the effects of LER on cross area uniformity. In other words, both rms and ξ in LER degrade device area variability with rms exhibiting the primary effect.

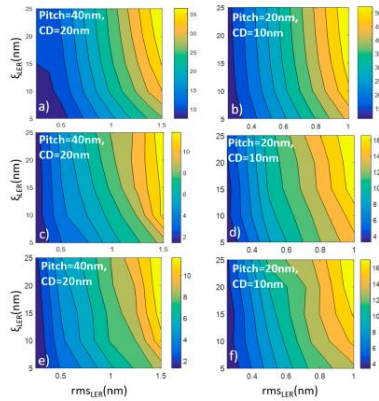


Figure 3. Contour plots of $\sigma(A)$ vs. rms_{LER} and correlation length L_{LER} . Left (a,c) and right (b,d,f) columns contain the plots for $CD = 20$ nm and $CD = 10$ nm, respectively. Furthermore, in the second (c,d) and third (e,f) row the calculations have been done considering patterns with correlated edges and correlated edges and lines respectively.

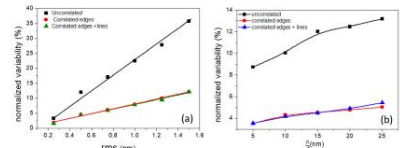


Figure 4. An example of the dependence of the normalized variability $\sigma(A)$ on (a) rms and (b) L for typical parameters. One can notice the linear and sublinear increase of $\sigma(A)$ vs. rms and L , respectively.

3.2. The Impact of Scaling Device Size

The comparison of the contour plots of the left and right columns reveals that the scaling down of pattern dimensions by a factor 2 (quadrupling of device density) is associated with an almost doubling of normalized area variability $\sigma(A)$. This observation holds at all rows, i.e., it is independent of the level of edge/line correlations.

3.3. The Impact of Edge and Line Correlations

When MP or DSA lithographic techniques are used for ReRAM pattern fabrication, edges and lines exhibit cross-correlations, i.e., they fluctuate in a correlated manner. The second and third rows of Figure 3 show the contour plots for $\sigma(A)$ when the pattern exhibits only edge and both edge and line correlations, respectively. Although the pattern of contour lines remain almost unaltered, the $\sigma(A)$ values demonstrate a clear reduction with respect to the values of first rows approximately by a factor 3. The amount of reduction is similar at the contour plots of the second and third rows, which indicates that the critical correlations for variability drop are those between edges. The cross-line correlations do not seem to play any role in LER-induced degradation effects on area uniformity.

3.4. Analytical Formula for LER Effects on Area Variability

The dependencies of $\sigma(A)$ on LER parameters found by modeling and shown in Figure 3 can be captured in an analytical formula which can be derived as follows: For patterns with smooth edges (no LER) the cross-point areas are fixed in all devices and equal to $A_i = CD_x CD_y$ with no variability at all. When we consider rough edges, LER induces local variability in line widths, which is usually called Line Width Roughness (LWR). Therefore, each crossing area can be roughly characterized by $A_i = CD_x CD_y$, where CD_x and CD_y are the average line widths across x - and y -directions enclosed in the i -th crossing area. Due to LER and LWR, CD_x and CD_y change randomly from area to area. If we assume that on average this variability is similar to both vertical and horizontal lines, we get for the $\sigma(A)$:

$$\sigma(A) = \frac{\text{std}(A_i)}{A_i} = \frac{\sqrt{2} \text{std}(CD)}{CD} \quad (2)$$

The relationship of CD variance ($\text{std}^2(CD)$) with local and total variances of LWR values has been studied extensively in LER literature and the following formula can be proven [20]:

$$\text{std}^2(CD) + \langle rms_{LWR}^2(CD) \rangle = rms_{LWR}^2(\text{total}) \quad (3)$$

where $rms_{LWR}^2(\text{total})$ is the rms value of LWR for the total lines included in model patterns, which assume to get sufficiently large lengths so that the rms_{LWR} value stabilizes at a fixed value, and $\langle rms_{LWR}^2(CD) \rangle$ is the mean variance of LWR calculated inside the segments of length CD , and averaged over all considered segments.

In order to get the relationship of $\sigma(A)$ with the input LER parameters, we need to pass from LWR to LER parameters. This can be achieved through the following formula connecting LWR and LER assuming similarity between left and right LER:

$$rms_{LWR}^2 = 2(1-c) rms_{LER}^2 \quad (4)$$

Here, c is the c-factor quantifying the cross-correlations between the left and right edges of lines. For totally uncorrelated edges, $c = 0$, whereas for fully correlated (anti-correlated), $c = 1 (-1)$ [26,33]. By combining (2), (3), and (4) we read:

$$\sigma(A) = \frac{\text{std}(A)}{A} \sqrt{(1-c)(rms_{LER}^2(\text{total}) - \langle rms_{LER}^2(CD) \rangle)} \quad (5)$$

The Formula (5) can be further processed in the case of edges with exponential autocorrelation functions (roughness exponent $\alpha = 0.5$) since for such edges it holds that

$$rms_{LER}^2(CD) = rms_{LER}^2(\text{total}) \left[1 - \frac{2\alpha}{CD} \left(1 + \frac{c}{2} e^{-\frac{CD}{L}} - 1 \right) \right] \quad (6)$$

Inserting (6) into (5) we get the final formula for the dependence of $\sigma(A)$ on LER parameters:

$$\sigma(A) = 2 \sqrt{2(1-c)} \frac{rms_{LER}}{CD} \frac{L}{CD} \sqrt{\frac{CD}{L} e^{-\frac{CD}{L}} - 1} \quad (7)$$

Equation (7) incorporates all the dependencies of normalized area variability on the dimensional parameters (CD), the principal LER parameters (rms_{LER} , L) and the level of edge correlations (c -factor). As expected from the numerical results, pitch and line correlations are not included since they have no impact. One can easily notice that the analytical Formula (7) predicts (a) the linear proportionality of $\sigma(A)$ to rms_{LER} , (b) the sublinear increase of $\sigma(A)$ with L , (c) the almost linear inverse proportionality impact of CD , and (d) the reduced effects of increased edge correlations on $\sigma(A)$ quantified by c through the factor $(1-c)$.

In order to get a more quantified and complete comparison of the analytical prediction with the numerical results, we show in Figure 5a a contour plot with the dependencies of $\sigma(A)$ on LER parameters (rms_L , L) as derived by the analytical Formula (7). We have chosen $c = 0$ (no edge correlations) and $CD = 20$ nm, which are the parameters of the numerical contour plot of Figure 3a. One can clearly identify the striking qualitative and quantitative similarity of two contour plots, which is more directly and quantitatively illustrated in Figure 5b where the difference of the numerical and analytical normalized variability $\sigma(A)$ is shown versus rms and L parameters. The difference is always very close to zero and justifies the predictive power of the analytical formula. The sole exception is for the small rms values lower than 0.5 nm where the analytical formula seems to underestimate the numerical results. However, the observed discrepancy is due to issues with the numerical results. More specifically, in order to simulate the real procedure where the LER effects are evaluated through the analysis of SEM images (see Figure 1), in the numerical modeling we pixelize the edge data by rounding the generated edge points on the generator algorithms. We have shown that this discretization (pixelization) process induces a noise impact on LER and causes an increase of the measured rms value as explained in [40]. Therefore, in these regimes with extremely small rms values, one should trust the predictions of the analytical Formula (7) more than the numerical results of the 2D modeling.

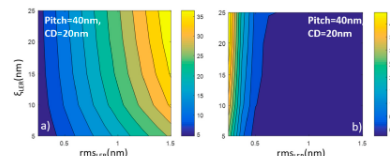


Figure 5. (a) Contour plot of the normalized variability $\sigma(A)$ cross-point area versus the LER parameters rms and L for $CD = 20$ nm and $c = 0$ (no edge correlations) and (b) the difference of numerical and analytical predictions for $\sigma(A)$ for the standard parameters $CD = 20$ nm and $c = 0$. One can notice the striking similarity of numerical and analytical results with the slight exception of very small rms values where numerical results are biased due to pixelization of edge data.

The similarity between numerical results and analytical predictions was confirmed independently of CD and edge correlations. This means that the Formula (7) comprises a strong analytical tool to get control and deeper understanding of the LER effects on ReRAM area variability and performance degradation since it captures successfully the impact of LER main parameters (rms_L , L) as well as of the line width (CD) and edge correlations which may come from different lithography steps used in pattern formation.

4. Conclusions

In this work, we model the effect of lithographic performance parameters on the operation of ReRAM devices, assuming the main three lithographic techniques: HLW, MP and DSA. According to our numerical model, it is found that both rms and L in LER degrade device area variability with rms exhibiting the primary effect. Additionally, it is found that edge correlations favor area uniformity while the normalized area variability is doubled when the size becomes half of the initial. For comparison, an analytical model was developed also to simulate the impact of lithography performance parameters. The comparison between the 2D numerical and the analytical one reveals that both provide the same results independently of CD and edge correlations. Nevertheless, the analytical model is more accurate at extremely small rms values. In this context, the developed numerical and analytical models are highly valuable predictive tools for the integration of ReRAM devices at very small technology nodes.

Author Contributions: Conceptualization, V.C., T.P., and P.D.; data curation, V.C., G.P., A.K., and T.P.; formal analysis, V.C.; funding acquisition, V.C.; investigation, V.C., G.P., P.K., A.K., T.P., and P.D.; methodology, V.C. and P.D.; project administration, V.C.; resources, A.K. and T.P.; software, V.C. and G.P.; supervision, V.C.; validation, V.C.; visualization, V.C., G.P., and P.K.; writing—original draft, V.C., P.K., T.P., and P.D.; writing—review & editing, V.C., T.P., and P.D.

Funding: For this research, V.C., G.P., and P.D. have received funding from the EMPER programme “3DNano” co-financed by the Participating States and from the European Union’s Horizon 2020 research and innovation programme. P.K. and P.D. gratefully acknowledge the financial support from the Greece–Russia bilateral joint research project MEM-4 (proj.no/MIS FAPF1-00030502467) and research project RADAR (proj.no/MIS T1EAK-02SP9XV2780) supported by CSRT and funded by National and European funds. Finally, the authors A.K. and T.P. wish to acknowledge the financial support of the Engineering and Physical Sciences Research Council (EPSRC) grants EP/K017829/1, EP/R024642/1.

Conflicts of Interest: The authors declare no conflict of interest.

References

- Stathopoulos, S.; Khaat, A.; Trapatsch, M.; Cortese, S.; Serb, A.; Valov, I.; Prodromakis, T. Multibit memory operation of metal-oxide bilayer memristors. *Sci. Rep.* **2017**, *7*, 17332. [CrossRef] [PubMed]
- Khaat, A.; Ayllón, F.; Prodromakis, T. High Density Crossbar Arrays with Sub-15 nm Single Cells via Liftoff Process Only. *Sci. Rep.* **2016**, *6*, 32614. [CrossRef]
- Wu, H.; Yao, P.; Gao, B.; Wu, W.; Zhang, Q.; Zhang, W.; Deng, N.; Wu, D.; Wong, H.-S.P.; Yu, S.; et al. Device and circuit optimization of RRAM for Neuromorphic computing. In Proceedings of the IEEE International Electron Devices Meeting (IEDM), San Francisco, CA, USA, 2–6 December 2017; pp. 11.5.1–11.5.4.
- Li, H.; Xu, X.; Yuan, P.; Dong, D.; Gong, T.; Liu, J.; Yu, Z.; Huang, F.; Zhang, K.; Hsu, C.; et al. BEOL Based RRAM with One Extra mask for Low Cost, Highly Reliable Embedded Application in 28 nm Node and Beyond. In Proceedings of the IEEE International Electron Devices Meeting (IEDM), San Francisco, CA, USA, 2–6 December 2017; pp. 2.4.1–2.4.4.
- Fujitsu Semiconductor Launches World’s Largest Density 4 Mbit ReRAM Product for Mass Production. 2016. Available online: <https://phys.org/news/2016-10-fujitsu-semiconductor-world-largest-density.html> (accessed on 10 December 2017).
- Gowonamu, B.; Kap, C.S.; Chen, Y.-Y.; Paraschiv, V.; Kubtsak, S.; Fantini, A.; Radu, I.; Goux, I.; Clima, S.; Degraeve, R.; et al. 10×10 nm² Hf/HfO₂ cross-point resistive RAM with excellent performance, instability and low-energy operation. In Proceedings of the International Electron Devices Meeting, Washington, DC, USA, 5–7 December 2011; pp. 31.6.1–31.6.4. [CrossRef]



Materials 2019, 12, 1922

11 of 12

7. Wang, A.; Lundström, M.; Chen, D.; Shi, M.; Shan, K.; Han, Y.; Hwangjima, T.; Adachi, K.K.; Mida, R.; Wang, R.; et al. Nanoscale carbon motion in GaN, HfO₂, and TiO₂ memristive systems. *Nat. Nanotechnol.* **2016**, *11*, 47–74. [CrossRef] [PubMed]

8. Luo, Q.; Xu, X.; Gong, T.; Li, H.; Dong, T.; Ma, H.; Yuan, P.; Gao, J.; Liu, J.; Yu, Z.; et al. 4-layer 3D Vertical ReRAM with Excellent Scalability towards Storage-Class Memory Applications. In Proceedings of the IEEE International Electron Devices Meeting (IEDM), San Francisco, CA, USA, 2–6 December 2017; pp. 27.3–27.4.

9. Sethi, A.; Hill, J.; Khatt, A.; Nordin, R.; Frodinowski, T. Unsupervised learning in probabilistic neural networks with multi-state metal-oxide memristive systems. *Nat. Commun.* **2016**, *7*, 12811. [CrossRef] [PubMed]

10. Sethi, A.; Khatt, A.; Frodinowski, T. Stochasticly Fused Digital-Analogue Reconfigurable Computing using Memristors. *Nat. Commun.* **2018**, *9*, 270. [CrossRef]

11. Chen, W.H.; Liu, W.J.; Liu, L.; Li, L.L.; Hua, C.H.; Liu, H.T.; Liu, H.L.; Yu, J.; Xu, Y.; Yu, S.S.; et al. A 3MB Dual-Matrix ReRAM Macro with Sub-Hit Computing-In-Memory and Memory Functions Enabled by Self-Write Termination Scheme. In Proceedings of the IEEE International Electron Devices Meeting (IEDM), San Francisco, CA, USA, 2–6 December 2017; pp. 24.2.1–24.2.4.

12. Libben, M.; Karakostas, P.; Ioannou-Sougleris, V.; Nomral, P.; Dimitrak, P.; Valos, I. Graphene-Modified Interface Controls Transition from VCM to ECM Switching Modes in Ta/TaO₂ Based Memristive Devices. *Adv. Mater.* **2018**, *30*, 1802007. [CrossRef]

13. Tsoukouras, M.; Boussoulas, P.; Aralinda, V.; Skoufias, E.; Tsoukalis, D. Ultra-Low Power Multilayer Switching with Enhanced Endurance by Forming Two TaO_x-based ReRAM with Interbedded Pt/Niobium. *Phys. Status Solid (a)* **2017**, *214*, 170070. [CrossRef]

14. Chen, A. Area and Thickness Scaling of Forming Voltage of Resistive Switching Memristors. *IEEE Trans. Electron Devices* **2014**, *61*, 51–59. [CrossRef]

15. Wong, H.S.P.; Lee, H.Y.; Yu, S.; Chen, Y.S.; Wu, Y.; Chen, P.S.; Lee, R.; Chan, F.T.; Tsai, M.J. Metal Oxide ReRAM. *Proc. IEEE* **2012**, *100*, 1951–1970. [CrossRef]

16. Fang, Z.; Li, X.; Wang, X.; Liu, A. Area Dependent Low Frequency Noise in Metal Oxide Based Resistive Random Access Memory. *Int. J. Inf. Electron. Eng.* **2012**, *2*, 882–884. [CrossRef]

17. Lee, J.; Park, J.; Jung, S.; Hwang, H. Scaling Effect of Device Area and Film Thickness on Electrical and Reliability Characteristics of ReRAM. In Proceedings of the IEEE International Nanoelectronics Technology Conference and Materials for Advanced Metallization (ICTMAM), Dresden, Germany, 9–12 May 2011. [CrossRef]

18. Hayakawa, Y.; Himeeno, A.; Yasuhara, R.; Boualart, W.; Vecchio, E.; Vandeweyer, F.; Witters, T.; Croiti, D.; Joutzak, M.; Fuji, S.; et al. Highly scalable TaO_x ReRAM with centralized filament for 28-nm embedded applications. In Proceedings of the Symposium on VLSI Technology Digest of Technical Papers, 174–175, Kyoto, Japan, 17–19 June 2015. [CrossRef]

19. Chen, H.J.; Chen, A.B.K.; Yang, X.; Chen, L.W. Fully Electronic Switching with High Uniformity, Resistance Tolerability, and Good Retention in Pt-Doped TaO_x Thin Films for ReRAM. *Adv. Mater.* **2011**, *23*, 3647–3652. [CrossRef]

20. Guan, W.; Long, S.; Liu, Q.; Liu, M.; Wang, W. Memristor Non-volatile Resistive Switching in Cu Doped ZnO. *IEEE Electron Device Lett.* **2008**, *29*, 434–437. [CrossRef]

21. Kim, M.; Choi, K.C. Transparent and flexible resistive random access memory based on Al₂O₃ film with multilayer electrodes. *IEEE Trans. Electron Devices* **2017**, *64*, 3906–3910. [CrossRef]

22. Yoon, K.J.; Kim, G.H.; Yoo, S.; Ba, W.; Yoon, J.H.; Park, T.H.; Kwon, D.E.; Kwon, V.J.; Kim, H.J.; Kim, Y.M.; et al. Double-Layer-Stacked One-Diode-One-Resistor Resistive Switching Memory Cross-point Array with an Extremely High Rectification Ratio of 10¹⁰. *Adv. Electron. Mater.* **2017**, *1*, 1700152. [CrossRef]

23. Sawa, A. Resistive switching in transition metal oxides. *Nature* **2008**, *455*, 20–26. [CrossRef]

24. Kim, H.-D.; An, M.-M.; Lee, E.R.; Kim, T.C. Stable Bipolar Resistive Switching Characteristics and Resistive Switching Mechanism Observed in Aluminum Nitride-based ReRAM Devices. *IEEE Trans. Electron Devices* **2011**, *58*, 3966–3973. [CrossRef]

25. Kim, H.-D.; Yun, M.E.; Hong, M.; Kim, T.C. Size-dependent resistive switching properties of the active region in nickel oxide-based cosubstituted array resistive random access memory. *J. Nanosci. Nanotechnol.* **2014**, *14*, 9088–9091. [CrossRef]

Materials 2019, 12, 1922

26. Constantinides, V.; Goggin, E.; Patis, G.P. Side-wall roughness in nanophotonic: Origin, evolution and device effects. *Nanophotonics*. In *The Art of Fabricating Nanoelectronic and Nanophotonic Devices and Systems*; Kishino, M., Ed.; Wiley: Hoboken, NJ, USA, 2019; pp. 461–497.

27. Wang, S.; Baker, J.A. Simulation Study of Gate-Less Edge Roughness Effects on Draping Profiles of Short-Channel MOSFET Devices. *IEEE Trans. Electron Devices* **2006**, *53*, 228–232. [CrossRef]

28. Wilkai, K.; Ueno, N.; Tagita, K. Influence of Interface Roughness on MOSFET devices with sub-30-nm gates. *Micron* **2004**, *35*, 463–473. [CrossRef]

29. Kato, S.; Hasebe, A.R.; Amano, A.; Mizutani, D.; Usami, T. Analysis of Statistical Fluctuations due to Line Edge Roughness in sub-100-nm MOSFETs. In *Simulation of Semiconductor Process and Device 2007*; Springer: Boston and Dordrecht, MA, USA, 2007; pp. 79–81.

30. Lee, D.; Kim, K.; Kim, C.; Kang, M.; Shin, H. Line Edge Roughness and Process Variation Effect of Three-Dimensional Al₂O₃ Nanowire MOSFET Devices. *J. Nanosci. Nanotechnol.* **2007**, *7*, 7130–7133. [CrossRef]

31. Barakat, E.; Jaradat, M.; Spruiell, N.; DiMayer, K.; Dink, A. Impact of LER and Random Output Fluctuations on Full-ET Matching Performance. *IEEE Trans. Nanotechnol.* **2008**, *7*, 249–256. [CrossRef]

32. Park, K.; Lee, F.H.; Spence, C.J. Low-Line Edge Roughness Model for Estimation of Full-ET Performance Variability. *IEEE Trans. Electron Devices* **2008**, *55*, 3059–3063. [CrossRef]

33. Constantinides, V.; Papanicolaou, G.; Goggin, E.; Patis, G.P.; Pothig, H.; Gatzelwald, K. Challenges in line edge roughness modeling on directed self-assembly lithography: placement errors and cross-line correlations. *J. Microelectromech. Syst.* **2017**, *26*, 1249–1261. [CrossRef]

34. Constantinides, V.; Goggin, E.; Roberts, J.; Stewart, J.K. Characterization and modeling of low-width roughness (LWR). *Micron* **2008**, *39*, 1227–1232. [CrossRef]

35. Mack, C.A. Generating random roughness, surfaces, and volumes. *Appl. Opt.* **1983**, *22*, 1472–1480. [CrossRef] [PubMed]

36. Constantinides, V.; Patis, G.P.; Ioannides, I.H.A.; Goggin, E. Line edge roughness and critical dimension variation: Physical characterization and comparison using model functions. *J. Vac. Technol. E: Microelectron. Nanotechnol.* **2008**, *22*, 1074. [CrossRef]

37. Constantinides, V.; Kulkarni, C.; Goggin, E.; Papanicolaou, G.; Patis, G.P. Effects of resist sidewall roughness on knowledge roughness reduction and transfer during etching in the most critical self-assembly technology. *J. Microelectromech. Syst.* **2018**, *27*, 1820. [CrossRef]

38. Palomares, G.; Kim, J. Effect of the form of the height-height correlation function on diffusion rate scattering from a self-affine surface. *Phys. Rev. E* **1998**, *58*, 3073–3077. [CrossRef]

39. ITRS. ITRS International Technology Roadmap for Semiconductors. Available online: <http://www.itrs.net/> (accessed on 10 December 2017).

40. Papanicolaou, G.; Constantinides, V. Line edge roughness measurement through SEM images: Effects of image digitization and their mitigation. *Proc. SPIE* **2007**, *10466*. [CrossRef]

© 2019 by the authors. Licensee MDPI, Basel, Switzerland. This article is an open access article distributed under the terms and conditions of the Creative Commons Attribution (CC BY) license (<http://creativecommons.org/licenses/by/4.0/>).

3.2. Διεθνής Συνέδρια

1. Evangelia Karagianni, Christina Lessi, “GaN wideband receiver for new generation applications”, Proceedings of the IIER International Conference, Bali, Indonesia, 30th -31st August, 2019.

GaN wideband receiver for new generation applications

Evangelia Karagianni, Christina Lessi
Hellenic Naval Academy, National Technical University of Athens
evka@hna.gr, christlessie@gmail.com

Abstract— *Socially critical applications such as wireless and satellite communications, terrestrial and flying radars, cable TV and intelligent transport infrastructure have a significant impact on our everyday lives. The combination of all modern technological applications is nowadays the interest of things (IoT). The IoT design that is presented is intended to be part of a transceiver, which will be placed in a hardware, offering better efficiency to new generation applications.*

Index Terms—Gallium Nitride technology, Internet of Things, Software Defined Network, Low Noise Amplifier.

1. INTRODUCTION

Upcoming applications such as 5G, IoT, autonomous vehicles have upgraded requirements such as higher power, enhanced functionality and lower cost. Consequently, the transceivers need redesign, including innovative solutions, since GaAs is no longer capable of meeting the new requirements [1].

GaN technology seems to be a good choice to replace GaAs, even though it is a relatively new technology, it has become very popular for its high frequencies or high power devices.

Comparing GaN technology with the older ones, such as Si and GaAs, the results are presented in Table 1 [2].

- 1) The power density of a GaN material is almost 10 times higher than Si material and it has good thermal conductivity.
- 2) GaN has 10 times higher breakdown field than Si or GaAs materials, so devices can be smaller with high impedances.
- 3) It has lower dielectric constant than other materials, resulting in a lower intrinsic junction capacitance. When parasitic such as output capacitance and layout inductances are reduced, switching losses are reduced too, resulting in a higher frequency operation with the same loss [3] [4].

- 4) GaN HEMT has the highest saturated electron velocity of about 2.7x10⁸ cm/s among other semiconductor transistors [2] [5].
- 5) GaN transistors have increased efficiency, smaller size and fast switching. The smaller size enables performance improvements in switching power applications.

Parameter	GaN	SiC	Ga As	Si
Band Gap (eV)	1.9	3.2	1.4	1.1
Practical Electron Mobility (cm ² /Vs)	1000	1000	1000	1000
Practical Hole Mobility (cm ² /Vs)	1000	1000	1000	1000
Practical Intrinsic Carrier Concentration (cm ⁻³)	10 ¹⁷	10 ¹⁷	10 ¹⁷	10 ¹⁷
Thermal Conductivity (W/mK)	1.5	3.9	0.7	1.5
Thermal Expansion Coefficient (10 ⁻⁶ /K)	5.5	5.5	6.5	2.6

Table 1. Comparative of GaN with other semiconductor materials.

II. WIDEBAND APPLICATIONS AND SUBSTRATE ARCHITECTURE

The technological revolution of the modern era enables the wireless communication system functions, from the antenna to the interface, to be executed and programmed by a single high level software language using a one hardware topology. These systems are the Software Defined Networks (SDN). An SDN has the ability to implement many different interfaces. However, since each standard can exploit a different frequency band, it is important the SDN to cover a large bandwidth.

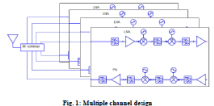


Fig 1. Multiple channel design

In order to achieve the wideband operation of the transceiver, its architecture will be based in multiple channels topology (Figure 1). In this case, each channel operates in a wide range of frequencies, but still different from the range of the other channels. The signal entering the antenna is driven by a digital switch on the appropriate channel. By using this architecture, it is easily achievable to increase the system capacity by adding more receiving and transmitting channels of different RF carriers [6].

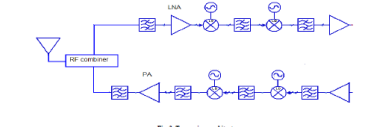
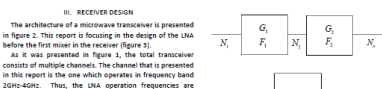


Fig 2. Transceiver architecture



The architecture of a microwave transceiver is presented in Figure 2. This report is focusing in the design of the LNA before the first mixer in the receiver (Figure 2). As it was presented in Figure 1, the total transceiver consists of multiple channels. The channel that is presented in this report is the one which operates in frequency band 20GHz-40GHz. Thus, the LNA operation frequencies are 20GHz-40GHz.

$$F_{system} = F_1 + \frac{F_2 - 1}{G_1} + \frac{F_3 - 1}{G_1 G_2} + \dots + \frac{F_n - 1}{G_1 G_2 \dots G_{n-1}} \quad (1)$$

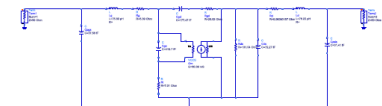


Fig 4. Series of microwave elements



Fig 5. Valid signal model of GaN HEMT with 170nm gate length and 2000V gate width at bias conditions of V_{GS} = 0V and V_{DS} = 2V

The paper is part of the RADAR project "Intelligent 3D Integration employing disruptive nanotechnologies for the next generation of smart power RF modules", project #17204-0029, with co-funding of Greece and European Union.

It is supported by the Hellenic Republic.



Με τη συγχρηματοδότηση της Ελλάδας και της Ευρωπαϊκής Ένωσης

GaN Wideband Receiver for New Generation Applications

The most important characteristic of an LNA is the low level of noise that adds in the signal. If the receiver is depicted as a set of boxes in a row (figure 4), each box represents an element of this receiver that has a gain and a noise level, then the total noise level is calculated by the equation 1. The equation explains that the noise of the first element is the most crucial for the total system noise, while the next elements noise is not that important since it is divided by the gain of all previous elements.

The receiver will be designed by using GaN technology. On figure 5 the small signal model of the GaN HEMT that will be used is presented [7]. Additionally, the S-parameters of the transistor are presented in figure 6.

The cascade topology will be used for the LNA design. The desision of that topology is based on the benefits that it offers according the output gain considering at the same time the low noise level [8]. The operation principles are these which was described in equation 1. Furthermore, the matching circuit will have two different parts: the first one is the 2GHz matching circuit and the second one is the 4GHz matching circuit. This topology operates as it presented in figure 7. The two matching circuits leads to the proper operation of the LNA in the frequencies between the edges. In figure 8 the complete LNA design is presented, while in figure 9 the noise figure and the S-parameters are presented.

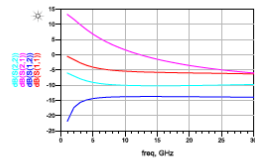


Fig. 6. S-parameters of GaN HEMT small signal model



Figure 7: Gain plots with two matching circuit design.

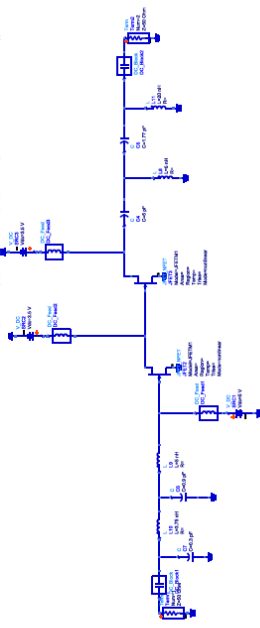


Fig. 8. The complete LNA design

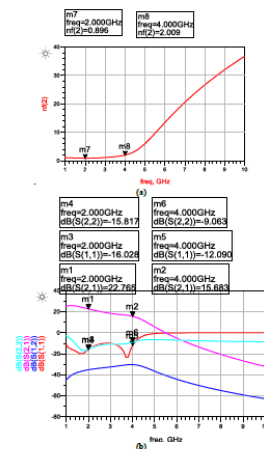


Fig. 9. a) Noise figure of figure 17 design, b) S-parameters of figure 17 design

IV. CONCLUSION

The LNA that was presented will be used in a wideband receiver. The simulation results show that its operation is suitable for this use, as the objectives were achieved: first the low noise operation, and second the high gain. Finally it is important to be mentioned that the LNA is unconditionally stable, as it results from the stability control equations.

REFERENCES

- [1] <http://www.ums-gas.com/cha6710-99f-a-new-gan-5w-mp-a.php>
- [2] S. Chen, B. Mulgrew, and P. M. Grant, "A clustering technique for digital communications channel equalization using radial basis function networks," *IEEE Trans. on Neural Networks*, vol. 4, pp. 570-578, July 1993.
- [3] Kiran Bernard, "Advantages of using Gallium Nitride FETs in satellite applications", *Renesas White Paper*, 2018
- [4] David Schaufner, Bror Peterson, "Gallium Nitride - A critical Technology for 5G", *Quorvo White Paper*, 2016
- [5] E. Karagianni, C. Lesi, C. Vasouras, "On-going GaN SSB for naval radar transmitters: a MMIC amplifier design", *9th International Conference on High-Performance Marine Vehicles*, 2014
- [6] Paul Burns, "Software defined Radio for 3G", 2003 Artech House, Inc.
- [7] Zhen Liu thesis: High Frequency Small-Signal Modelling of GaN High Electron Mobility Transistors for RF applications
- [8] C. Lesi, E. Karagianni, "An X-Band Low Noise Amplifier design for marine navigation radars", *Int. J. Communications, Network and System Sciences*, 2014



ΕΛΛΗΝΙΚΗ ΔΗΜΟΚΡΑΤΙΑ
ΥΠΟΥΡΓΕΙΟ
ΟΙΚΟΝΟΜΙΑΣ & ΑΝΑΠΤΥΞΗΣ
ΕΙΔΙΚΗ ΓΡΑΜΜΑΤΕΙΑ ΕΠΑ & ΤΕ
ΕΙΔΙΚΗ ΥΠΗΡΕΣΙΑ ΔΙΑΧΕΙΡΙΣΗΣ ΕΠΑ-ΕΚ

ΕΠΑ-ΕΚ 2014-2020
ΕΠΙΧΕΙΡΗΣΙΑΚΟ ΠΡΟΓΡΑΜΜΑ
ΑΝΤΑΓΩΝΙΣΤΙΚΟΤΗΤΑ
ΕΠΙΧΕΙΡΗΜΑΤΙΚΟΤΗΤΑ
ΚΑΙΝΟΤΟΜΙΑ

ΕΣΠΑ
2014-2020
ανάπτυξη - εργασία - αλληλεγγύη

Με τη συγχρηματοδότηση της Ελλάδας και της Ευρωπαϊκής Ένωσης



4. Παρουσιάσεις σε διεθνείς επιστημονικές συναντήσεις

1. Συμμετοχή στο 40th TCM CapTech Meeting, 17 Σεπτεμβρίου 2018, EDA, Βρυξέλλες, Παρουσίαση του PANTAP

40th TCM CapTech Meeting
September 17 2018; EDA, Brussels, BE

Hellenic Naval Academy (HNA) – Ministry of National Defense – Hellenic Republic

Evangelia Karagianni
Associate Professor
Electronics Laboratory Director
Hellenic Naval Academy

ΣΧΟΛΗ ΝΑΥΤΙΚΩΝ ΔΟΚΙΜΩΝ
HELLENIC NAVAL ACADEMY www.hna.gr

FORTH
INSTITUTE OF ELECTRONIC STRUCTURE AND LASER

HNA Projects
RADAR: "Heterogeneous Three-dimensional Integration using innovative nanotechnologies for the new generation of microwave power transceivers"

- EU, Action for Research, "Research - Creation - Innovation", 2014-2020, Operational Program "Competitiveness-Entrepreneurship-Innovation"
- The project has three years duration (from now), seven institutions cooperate and the coordinator is the Foundation for Research and Technology (FORTH) of Crete.
- The Hellenic Naval Academy as a partner has to design and optimize the GaN MMIC circuits: the High Power Amplifier (HPA) and the Low Noise Amplifier (LNA).
- Modeling will be done using electronic design and electromagnetic simulation software such as ADS, HFSS, EMPro and CST to achieve optimization of performance. The design library will be completed in parts through a sufficient number of feedback cycles to design, construct, characterize and compare between computational and experimental data.

MEMS membrane
GaN/SiC substrate ~500µm
Metallic Platform

RADAR : MRG/FORTH Innovation: COPLANAR Approximation (CP)

Coplanar Approximation (IESL Innovation)

1. HPA & LNA Construction (20 fabrication steps)
2. RF MEMS & Air-Bridge Interconnect (7 fabrication steps)

Total fabrication steps: 27
Without backside processing
Higher yield & better circuits
mechanical reliability

Microstrip Approximation (Existing Technology)

1. HPA & LNA Construction (20 fabrication steps)
2. substrate thinning (3 high "risk" and cost fabrication steps)
3. Vias & Au metal Via filling process (6 high "risk" and cost fabrication steps)
4. RF MEMS & Air-Bridge Interconnect (7 fabrication steps)

Total fabrication steps: 36

RADAR

- The 1st Prototype (GaN/SiC) will operate at X-band (8-12 GHz) with 50W output power
 - The T/R of this category mainly targets the purchase of radar for ground-based marine and flying applications.
 - This market requires a relatively small number of T/R (~ 1000 / radar), but the cost of each can be as high as 200-300 €, it is a performance driven application.
- The 2nd Prototype (GaN/Si) will operate at Ka-band (26-40 GHz) with 30W output power and with the required thermal support.
 - HPA:** The current state of commercial products is that high output power (over 40W) is provided in zones L and C. In zone X the highest power value is 35W while in zone Ka the value is 15W. In general, commercial products are produced using the microstrip technique.
 - "RADAR": The first HPAs will be produced with coplanar technique with 50W power in X-band and 30W in Ka Band.
 - LNA:** Commercial products are up to 22GHz with a noise figure (NF) of 2.5dB.
 - "RADAR": Coplanar LNA with SotA performance will be produced. The emphasis will be on the Ka band targeting NF <1.7dB.

2. E. Καργιάννη "State of the Art Ka-band MMICs using Stripline & Coplanar Techniques in Filters & GaN/Si High Power Amplifiers Design", Συμπόσιο Επιστήμης & Τεχνολογίας, ΛΑΕΔ, ΥΠΕΘΑ (ΓΔΑΕΕ-ΔΑΕΤΕ) Science & Technology Symposium, Oct. 22-23, 2018



ΕΛΛΗΝΙΚΗ ΔΗΜΟΚΡΑΤΙΑ
ΥΠΟΥΡΓΕΙΟ
ΟΙΚΟΝΟΜΙΑΣ & ΑΝΑΠΤΥΞΗΣ
ΕΙΔΙΚΗ ΓΡΑΜΜΑΤΕΙΑ ΕΠΑ & ΤΕ
ΕΙΔΙΚΗ ΥΠΗΡΕΣΙΑ ΔΙΑΧΕΙΡΙΣΗΣ ΕΠΑΝΕΚ

ΕΠΑΝΕΚ 2014-2020
ΕΠΙΧΕΙΡΗΣΙΑΚΟ ΠΡΟΓΡΑΜΜΑ
ΑΝΤΑΓΩΝΙΣΤΙΚΟΤΗΤΑ
ΕΠΙΧΕΙΡΗΜΑΤΙΚΟΤΗΤΑ
ΚΑΙΝΟΤΟΜΙΑ

ΕΣΠΑ
2014-2020
ανάπτυξη - εργασία - αλληλεγγύη



Με τη συγχρηματοδότηση της Ελλάδας και της Ευρωπαϊκής Ένωσης

State of the Art Ka-band MMICs using Stripline & Coplanar Techniques in Filters & GaN/Si High Power Amplifiers Design

Ευαγγελία Καραγιάννη
Associate Professor

Electronics Laboratory Director
Hellenic Naval Academy
Ministry of National Defense
Hellenic Republic

ΣΧΟΛΗ ΝΑΥΤΙΚΩΝ ΔΟΚΙΜΩΝ
HELLENIC NAVAL ACADEMY
www.hnaa.gr

Electronics Laboratory - HNA
Combat Systems, Naval Operations, Sea Studies,
Navigation, Electronics & Telecommunications Sector

Research Interests

- Monolithic Microwave Integrated Circuits (Design and Optimization)
- Microwave microstrip-stripline filters up to 40 GHz (ADS)
- Microwave Power Amplifiers and Microwave Low Noise Amplifiers in MIC and MMIC technologies (ADS)
- Microstrip Antennas (HFSS-CST)
 - Millimeter Wave Circuit Design
 - Ultra WideBand Applications
 - Metamaterials

Collaborations

- Marine Materials Laboratory – Mechanics and Materials Sector – HNA
- Microelectronics Group – Institute of Electronic Structure and Laser - Foundation of Research and Technology – Hellas (MRG/FORTH)
- Microwaves and Fiber Optics Laboratory - Institute of Communication and Computer Systems - School of Electrical and Computer Engineering - National Technical University of Athens
- Electronics Laboratory – Department of Informatics and Telecommunications – National and Kapodistrian University of Athens
- Intracom Defense Electronics
- Prisma Electronics
- Institute of Nanoscience and Nanotechnology (INN) - Research Centre for Nuclear Research - Demokritos

Filters

State of the Art Ka-band MMICs using Stripline Techniques in Filter Design

- Determining the type and order of approximation functions to be used.
- Finding the corresponding low-pass prototype.
- Transforming the low-pass network into a bandpass configuration.
- Transforming the lumped element into distributed elements.

Elliptic bandpass filters show lower loss and better selectivity than Chebyshev filters that have an equal number of resonators. So, they are well suited for microstrip applications. However, because of the difficulty in realizing practical impedance levels, elliptic bandpass filters are not widely used in microstrip.

Since Chebyshev filter has better roll-off than other filter types, this type of filter is chosen. The filter is designed by following the steps:

Stipline BandPass Filter Design

Specifications

Frequency (GHz)	Loss(dB)
31.3 - 31.8	>51
31.8 - 35.5	>30
37 - 40	<2 (passband)
41.5 -	>30

5th order Chebyshev BPF (lumped elements)

Ideal Coupled Transmission Lines

- Use equations for designing stripline BPF with N + 1 coupled line sections:
 - For 1st coupling: $Z_1 = \frac{Z_0}{2}$
 - For intermediate coupling: $Z_n = \frac{Z_0}{2} \sqrt{\frac{1 - \epsilon_r}{1 + \epsilon_r}}$
 - For final coupling: $Z_N = \frac{Z_0}{2}$

Then we obtain even and odd mode characteristic impedances:

$$Z_{oe} = Z_0[1 + jZ_0 + (Z_0)^2]$$

$$Z_{oo} = Z_0[1 - jZ_0 + (Z_0)^2]$$

Stripline filter 5th Order (0.75mm)

- Calculation of the physical parameters of the coupled stripline components according to:
 - the technology and
 - the odd and even impedances

Design & Layout

Stripline BandPass Filter

Amplifiers

State of the Art Ka-band MMICs using Coplanar Techniques in GaN/Si High Power Amplifiers Design

- GaN technology is a relatively new technology compared to other semiconductors, such as Si and GaAs, but the technology of choice for high frequency applications requiring higher energy and/or higher operating frequency is rapidly becoming available, such as long distance signal transmission or at high power (eg radar, base station transceiver, D-TS, satellite communications, electronic interference -EMI and jamming, etc.).
- This technology, albeit new, already has dynamic entry into the markets. The adoption of GaN will ultimately lead to lower costs because:
 - (1) the complexity of the circuits is simplified
 - (2) the cost / watt is drastically reduced
 - (3) the operation time of the system is reduced because GaN devices require less energy and maintenance due to the durability of the material under adverse conditions (eg high temperatures).
- The new technology considered to be the successor of the circulator switches are the high-frequency microelectronic switches (RF MEMS) which at a typical operating frequency of 10GHz exceed:
 - (a) input losses to 1dB instead of 0.8;
 - (b) M isolation (40dB instead of 37);
 - (c) to have a smaller trace to go 5mm2 instead of 1.5x5 mm2) and lower power consumption (RF MEMS switches have zero consumption).
- Lower-volume devices that operate at much higher power levels will encounter serious problems with increased levels of heat dissipation. The solution for future TIR (with better performance, less trace and volume and at a lower cost) is the combined use of GaN and RF MEMS supported by an efficient platform for removing the heat produced

Power Amplifiers

Two types of radars on ships importance

- >S-Band
- >X-Band

- threat detection
- precipitation tracking
- maritime vessel traffic management

Power Amplifiers

- > the most expensive MMIC in navigation radars
- > improve the performance

Amplifier Technologies

- high power tubes
 - > Magnetron
 - > Traveling Wave Tubes
 - > Klystrons
 - > Gyrotrons
- solid state amplifiers using silicon or GaAs

the next generation of these systems: gallium nitride (GaN) devices

- low power output
- Phased Array systems
- Continuous-Wave Low Probability of Interception (LPI) systems

Advances of GaN Technology

- The most common technology to replace GaAs is that of GaN due to a variety of superior material properties such as:
 - High energy gap (3.4eV),
 - High critical electric field,
 - Higher load density and
 - High thermal conductivity.
- Support high power applications and hence a smaller circuit area for the same performance.
- A higher electron speed allows signal amplification at higher frequencies.
- GaN circuit devices can respond to the increased demands of future TIRs for:
 - greater power (over 40dBm),
 - lower noise and higher operating frequency

the system benefits

- at cost,
- at range and
- volume

GaN Technology

GaN market strategies

GaN-on-SiC and GaN-on-Silicon market strategies



ΕΛΛΗΝΙΚΗ ΔΗΜΟΚΡΑΤΙΑ
ΥΠΟΥΡΓΕΙΟ
ΟΙΚΟΝΟΜΙΑΣ & ΑΝΑΠΤΥΞΗΣ
ΕΙΔΙΚΗ ΓΡΑΜΜΑΤΕΙΑ ΕΠΑ & ΤΕ
ΕΙΔΙΚΗ ΥΠΗΡΕΣΙΑ ΔΙΑΧΕΙΡΙΣΗΣ ΕΠΑ-ΕΚ

ΕΠΑ-ΕΚ 2014-2020
ΕΠΙΧΕΙΡΗΣΙΑΚΟ ΠΡΟΓΡΑΜΜΑ
ΑΝΤΑΓΩΝΙΣΤΙΚΟΤΗΤΑ
ΕΠΙΧΕΙΡΗΜΑΤΙΚΟΤΗΤΑ
ΚΑΙΝΟΤΟΜΙΑ

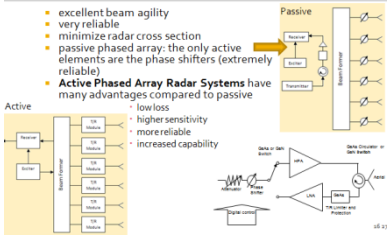
ΕΣΠΑ
2014-2020
ανάπτυξη - εργασία - αλληλεγγύη

Με τη συγχρηματοδότηση της Ελλάδας και της Ευρωπαϊκής Ένωσης



Phased Array Radars

- excellent beam agility
- very reliable
- minimize radar cross section
- passive phased array: the only active elements are the phase shifters (extremely reliable)
- Active Phased Array Radar Systems have many advantages compared to passive
 - low loss
 - higher sensitivity
 - more reliable
 - increased capability

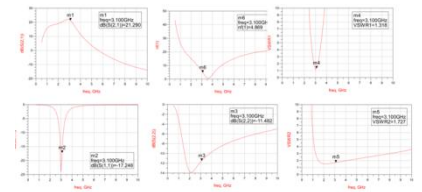


GaN solid state amplifier design in the S-band 2.9-3.1 frequency region

- The TGF2033-02 is a discrete 1.25mm GaN on SiC HEMT which operates from DC-38 GHz.
- Provides 38 dBm of saturated output power with power gain of 28 dB at 3 GHz.
- The maximum power added efficiency has a typical value of 45% and a maximum value of 60% which makes the TGF2033-02 appropriate for high efficiency applications.
- Simulation target: GaN 20dB, 21.5dB, 52.2dB, VSWR<1.5, Wideband Stability.

The circuit diagram shows a GaN HEMT amplifier with an input matching circuit, an intermediate matching circuit, and an output matching circuit. The design aims to compromise between high gain and low noise figure, reduce reflections between stages, and ensure maximum power transmission.

Simulation Results



RADAR Project: "Heterogeneous Three-dimensional Integration using innovative nanotechnologies for the new generation of microwave power transceivers"

- EU Action for Research, "Research - Creation - Innovation", 2014-2020, Operational Program "Competitiveness-Entrepreneurship-Innovation"
- The project has three years duration (from now), seven institutions cooperate and the coordinator is the Foundation for Research and Technology (FORTI) of Crete.
 - Prisma Electronics
 - Global Nanotechnologies
 - Institute of Nanoscience and Nanotechnology "Demokritos"
 - National and Kapodistrian University of Athens
 - Hellenic Naval Academy
 - AMEN Technologies
- The Hellenic Naval Academy as a partner has to design and optimize the GaN MMIC circuits: the High Power Amplifier (HPA) and the Low Noise Amplifier (LNA).
- Modeling will be done using electronic design and electromagnetic simulation software such as ADS, HFSS, EMPro and CST to achieve optimization of performance. The design library will be completed in parts through a sufficient number of feedback cycles to design, construct, characterize and compare between computational and experimental data.

HNA Projects

- Wireless and satellite communications, terrestrial and airborne radar, cable TV, intelligent transport infrastructure and the Internet of Things (IoT) are socially critical applications that have a significant impact on our everyday lives.
 - All these applications are based on the use of transceivers (T/R) that allow the emission of electromagnetic (EM) waves.
 - The central element of the transceiver is the RF front end or Low Noise Block which is composed of -among others-
 - high power amplifiers (HPAs) for signal transmission,
 - low power amplifiers (LNAs) for reception of the signal,
 - a common transmit / receive antenna and
 - a switch that allows the transition from the transmitting circuit to the corresponding receive.
-
- The diagram shows a cross-section of a GaN substrate with a silicon interposer, illustrating the heterogeneous three-dimensional integration.

T/R Re-designation: Demand

- The current industrial technology of the HPA "Output" Circuit (and "Input" LNA circuit) is based on GaAs semiconductor arrays that are hybridized to the antenna via a switching system (circulator switch) capable of electromagnetic (E/M) isolation.
 - Upcoming applications such as 5G, IoT, autonomous vehicles, new generation active phase antenna radar have upgraded requirements such as
 - higher power,
 - higher operating frequency,
 - smallest footprint and volume,
 - enhanced functionality and
 - lower cost
 - What is also worth mentioning is the attempt to exploit the terahertz gap that is now unutilized, which will soon require reliable T/R.
 - Consequently, transceivers need redesigning and introducing innovative solutions since GaAs and circulator switches are no longer capable of meeting the new requirements.
-
- The diagram shows a T/R module with an input matching circuit, a switch, and an output matching circuit.

RADAR Prototypes

- 1st Prototype (GaN/SiC)
 - X-band (8-12 GHz) operation with 50W output power. It will be demonstrated to a 8-element phased array system. Because of the high power, an innovative thermal platform will be developed based on Thermal Interface Materials-TIM as well as Thermo Electric Cooling-TEC, 3D integrated with the T/R.
- 2nd Prototype (GaN/Si)
 - Operate at Ka-band (26-40 GHz) with 30W output power and the corresponding thermal support

Hellenic Naval Academy Participation in RADAR

- Leader WP 2.2: Design Library for the HPA & LNA
 - For the performance optimization of the GaN MMIC circuits such as HPA, the modeling will be done using Electronic and Electromagnetic Software like ADS, HFSS, EMPro και CST. The design library will be completed in part through a sufficient number of feedback cycles to design, construct, characterize and compare computational and experimental data
- Participation in
 - WP 2.4: Surface acoustic wave GaN sensor
 - WP 2.6: Si interposer (Modeling and Optimization of the Through Silicon Vias -TSV structures that will serve as vertical vectors of the RF signal through the silicon interposer of the prototypes)
 - WP 4.1: Prototypes Design (RF, mechanical and thermal design for the metallic platform that will have the 4 or 8 T/R modules)

Hellenic Naval Academy Participation in RADAR

- Leader WP 2.2: Design Library for the HPA & LNA
 - For the performance optimization of the GaN MMIC circuits such as HPA, the modeling will be done using Electronic and Electromagnetic Software like ADS, HFSS, EMPro και CST. The design library will be completed in part through a sufficient number of feedback cycles to design, construct, characterize and compare computational and experimental data
- Participation in
 - WP 2.4: Surface acoustic wave GaN sensor
 - WP 2.6: Si interposer (Modeling and Optimization of the Through Silicon Vias -TSV structures that will serve as vertical vectors of the RF signal through the silicon interposer of the prototypes)
 - WP 4.1: Prototypes Design (RF, mechanical and thermal design for the metallic platform that will have the 4 or 8 T/R modules)

RADAR Prototypes

- The current state of commercial HPAs is that high output power (over 40W) is provided in zones L and C. In zone X the highest power value is 35W while in zone Ka the value is 15W. In general, commercial products are produced using the microstrip technique.
 - The first HPA will be produced with the coplanar technique with 50W power at X-band and 30W at Ka Band.
- The current commercial LNAs are up to 22GHz with noise figure (NF) 2.5dB.
 - Coplanar LNA with SotA performance will be produced. The emphasis will be on the Ka band targeting NF <1.7dB.

Properties	State-of-the-art		RADARs	
	1 st Prototype	2 nd Prototype	X-Band	Ka-Band
Frequency				
Output Power (T)			50 W	35 W
Linear Gain (T)			21.4 dB	20.4 dB
Noise Figure (R)			1.7 dB	<2 dB
Linear Gain (R)			23 dB	23 dB

X-band (50W) T/R:

- The T/R of this category mainly targets the purchase of radar applications. According to a new Market Research Report "Purchasing Air Traffic Control Equipment" published by Markets and Markets (world leading market research firm), the global Traffic Control Equipment (ATC) market is expected to reach 5519.5M by 2020.
- This market demands relatively small number of T/R (-1000/radar) but the cost of every T/R may be reach 200-300€, so it is a performance driven application.
- The positive outcome will depend on:
 - (1) the transition of radar technology from today's brick technology to the predicted type of tile technology; and
 - (2) whether the new European safety standards RECAT-EU 2 and RECAT-EU3 requiring new technology, will be implemented based on the projected timeframe, i.e. 2020-21 in the 1st and 2022-23 in the 2nd.

Ka-band (30W) T/R:

- T/R of this type is mainly aimed at cost-driven applications such as wireless communications (5G), satellite communications (SATCOM), stand-alone vehicles, satellite and cable TV and IoT. Purchases of RF GaN-based devices require a very large number of T/R (cost-driven).
- A crucial factor in the commercial exploitation of these T/R will also be the time option to implement new standards in applications such as wireless communication (5G) expected for 2023 and the next generation SATCOM (2022).
- Especially for 5G, an important factor will be the final choice of frequencies that with the international designs so far favors the choice of Ka band.
- "Unique Business Window Opportunity" because many and large companies produce power transceivers but there is none to supply monolithic integrated, parameterized - "smart" transceivers.

Thank you for your attention



Ευρωπαϊκή Ένωση
Ευρωπαϊκό Ταμείο
Περιφερειακής Ανάπτυξης

ΕΛΛΗΝΙΚΗ ΔΗΜΟΚΡΑΤΙΑ
ΥΠΟΥΡΓΕΙΟ
ΟΙΚΟΝΟΜΙΑΣ & ΑΝΑΠΤΥΞΗΣ
ΕΙΔΙΚΗ ΓΡΑΜΜΑΤΕΙΑ ΕΠΑ & ΤΣ
ΕΙΔΙΚΗ ΥΠΗΡΕΣΙΑ ΔΙΑΧΕΙΡΙΣΗΣ ΕΠΑ-ΕΚ

ΕΠΑ-ΕΚ 2014-2020
ΕΠΙΧΕΙΡΗΣΙΑΚΟ ΠΡΟΓΡΑΜΜΑ
ΑΝΤΑΓΩΝΙΣΤΙΚΟΤΗΤΑ
ΕΠΙΧΕΙΡΗΜΑΤΙΚΟΤΗΤΑ
ΚΑΙΝΟΤΟΜΙΑ

ΕΣΠΑ
2014-2020
ανάπτυξη - εργασία - αλληλεγγύη

Με τη συγχρηματοδότηση της Ελλάδας και της Ευρωπαϊκής Ένωσης



5. Προβολή σε Μέσα Κοινωνικής Δικτύωσης και Εταιρικές Ιστοσελίδες

1. Προβολή του έργου και της εξέλιξης του στα Μέσα Κοινωνικής Δικτύωσης.

Prisma Electronics
@prismaelectronics

Αρχική σελίδα
Πληροφορίες
Φωτογραφίες
Κριτικές
Βίντεο
Δημοσιεύσεις
Εκδηλώσεις
Κοινότητα
Δημιουργήστε Σελίδα

Σας αρέσει ▾ Ακολουθείτε ▾ Κοινοποίηση

Επικοινωνήστε μαζί... Στείλτε μήνυμα

5.0 5 στα 5 - Βάσει της άποψης 8 απόψεων

Κοινότητα Προβολή όλων

Προσκαλέστε τους φίλους σας να δηλώσουν ότι τους αρέσει αυτή η Σελίδα

Αρέσει σε 2.859 άτομα

2.880 άτομα ακολουθούν αυτή τη Σελίδα.

Ιορδάνης Νηδελης and 13 ακόμη φίλοι like this or have checked in

45 κοινοποιήσεις παρουσίας

Πληροφορίες Προβολή όλων

Democratias Avenue 87
68132 Αλεξανδρούπολη
Λήψη οδηγίων
2551 035013
Αποστολή μηνύματος
www.prismaelectronics.eu
Κατάστημα υπολογιστών · Βιομηχανική εταιρεία
Impressum
Προτείνετε διορθώσεις

Διαφάνεια Σελίδας Δείτε περισσότερα

Το Facebook δείχνει πληροφορίες για να σας βοηθήσει να κατανοήσετε καλύτερα ποιος είναι ο σκοπός μιας Σελίδας. Δείτε τις ενέργειες που κάνουν τα άτομα που διαχειρίζονται και δημοσιεύουν περιεχόμενο.

Ημερομηνία δημιουργίας Σελίδας - 6 Απριλίου 2011

Σχετικές Σελίδες

Εσείς και 5 ακόμη

Μου αρέσει! Σχόλιο Κοινοποιήστε



ΕΛΛΗΝΙΚΗ ΔΗΜΟΚΡΑΤΙΑ
ΥΠΟΥΡΓΕΙΟ
ΟΙΚΟΝΟΜΙΑΣ & ΑΝΑΠΤΥΞΗΣ
ΕΙΔΙΚΗ ΓΡΑΜΜΑΤΕΙΑ ΕΠΙΧΕΙΡΗΣΙΑΚΩΝ
ΕΠΙΧΕΙΡΗΣΙΑΚΩΝ ΠΡΟΓΡΑΜΜΑΤΩΝ

ΕΠΙΧΕΙΡΗΣΙΑΚΟ ΠΡΟΓΡΑΜΜΑ
ΑΝΤΑΓΩΝΙΣΤΙΚΟΤΗΤΑ
ΕΠΙΧΕΙΡΗΜΑΤΙΚΟΤΗΤΑ
ΚΑΙΝΟΤΟΜΙΑ

ΕΣΠΑ
2014-2020
ανάπτυξη - εργασία - αλληλεγγύη

Με τη συγχρηματοδότηση της Ελλάδας και της Ευρωπαϊκής Ένωσης



Σελίδα Κέντρ... Εισερχ... Creator Studio Manage Jobs Ειδοπ... Περισσότερα... Επεξε... Ρυθμί... Βοήθεια



Prisma Electronics
@prismaelectronics

- Αρχική σελίδα
- Πληροφορίες
- Φωτογραφίες
- Κριτικές
- Βίντεο
- Δημοσιεύσεις**
- Εκδηλώσεις
- Υπηρεσίες
- Κατάστημα
- Ομάδες
- Σημειώσεις
- Προσφορές
- Θέσεις εργασίας
- Κοινότητα

Προώθηση

Επισκεφτείτε το Κέντρο Διαφημίσεων

Σας αρέσει... Ακολουθήστε... Κοινοποίηση... Επικοινωνήστε μαζί μας

Prisma Electronics
Δημοσιεύτηκε από Dimosthenis Karageorgiou (·) · 29 Νοεμβρίου 2019 ·

The Radar project consortium held its third plenary meeting in Athens, on the day 29 of November 2019.

The meeting took place in the Institute of Nano science and Nanotechnology at Athens.

The partners presented the main outcomes from the work packages so far, discussed and agreed on the most relevant questions, worked together on specific topics, made a general assessment of the project and planned the next steps.

More info for Radar project at <https://radar-project.iesl.forth.gr/>



Προώθηση Δημοσίευσης


Εσείς και 2 ακόμη

Μου αρέσει! Σχόλιο Κοινοποιήστε

Αναζητήστε δημοσιεύσεις σε αυτή τη :
Ελληνικά - English (US) - Shqip - Español - Português (Brasil)
Πληροφορίες για τα στατιστικά στοιχεία Σελίδων
Απόρρητο - Όροι - Διαφήμιση - Οι Διαφημίσεις μου
Cookies - Περισσότερα - Facebook © 2020

<https://www.prismaelectronics.eu/index.php/en/profil-en/news-en/186-the-radar-project-consortium-held-its-third-plenary-meeting-in-athens>

HOME PROFILE NEWS THE RADAR PROJECT CONSORTIUM HELD ITS THIRD PLENARY MEETING IN ATHENS



HOME PROFILE ACTIVITIES SOLUTIONS CONTACT Search

The Radar project consortium held its third plenary meeting in Athens

WRITTEN ON 29 NOVEMBER 2019



The Radar project consortium held its third plenary meeting in Athens, on the day 29 of November 2019.

The meeting took place in the Institute of Nano science and Nanotechnology at Athens.

The partners presented the main outcomes from the work packages so far, discussed and agreed on the most relevant questions, worked together on specific topics, made a general assessment of the project and planned the next steps.

More info for Radar project at <https://radar-project.iesl.forth.gr/>